Recent Advances on Surface Ground Deformation Measurement by means of Repeated Space-borne SAR Observations

C. Prati, A. Ferretti, D. Perissin

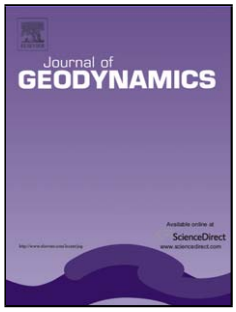

Title: Recent Advances on Surface Ground Deformation Measurement by means of Repeated Space-borne SAR Observations

Authors: C. Prati, A. Ferretti, D. Perissin

PII: S0264-3707(09)00144-6
DOI: doi:10.1016/j.jog.2009.10.011
Reference: GEOD 949

To appear in: *Journal of Geodynamics*

Received date: 10-2-2009
Revised date: 15-10-2009
Accepted date: 29-10-2009

Please cite this article as: Prati, C., Ferretti, A., Perissin, D., Recent Advances on Surface Ground Deformation Measurement by means of Repeated Space-borne SAR Observations, *Journal of Geodynamics* (2008), doi:10.1016/j.jog.2009.10.011

Recent Advances on Surface Ground Deformation Measurement by means of Repeated Space-borne SAR Observations

C. Prati[a,*], A. Ferretti[b], D. Perissin[a]

[a] *Dipartimento di Elettronica e Informazione, Politecnico, Piazza L. Da Vinci 32, 20133, Milano, Italy*

[b] *Tele-Rilevamento Europa – T.R.E. S.r.l.,Via. V. Colonna 7, 20149, Milano, Italy*

Abstract

Space-borne Synthetic Aperture Radar Interferometry (INSAR) is a well known widely used remote sensing technique to get precise (sub centimetric) surface deformation measurements on large areas (thousands of km^2) and high spatial density of measurement points (hundreds per km^2). In this work the recent technological advances of this technique are presented. First, a short review of the INSAR basics is dedicated to readers who are not INSAR specialists. Then, an analysis of the improvement of ground motion measurement offered by multiple repeated space-borne SAR observations gathered by the new generation of high resolution SAR systems is given. An example obtained with the recent German TERRASAR-X system is shown and compared with the measurements obtained with the elder C-Band RADARSAT-1 system. Finally, a possible processing of multi-temporal analysis of SAR images that allow extracting ground motion information also from partially coherent targets is given. In this case the core idea is to relax the restrictive conditions imposed by the Permanent Scatterers technique. The results obtained in different test-sites show an increased spatial density of areal deformation

* Corresponding author.
E-mail address: prati@elet.polimi.it

trend measurements, especially in extra-urban areas at the cost of missing motions with strong velocity variation.

Keywords: Synthetic Aperture Radar (SAR); INSAR; Permanent Scatterers; ground deformation.

1. Introduction

Synthetic Aperture Radar (SAR) Interferometry (*Bamler et al. 1998*) is based on the phase comparison of SAR images, gathered simultaneously or at different times with slightly different looking angles from space or airborne platforms. The phase of a SAR image contains the superposition of many terms including the distance of the radar from the illuminated targets on the ground. The phase difference of 2 SAR images gathered at different times contains a phase term proportional to the target motion occurring along the sensor-target Line-of-Sight (LOS) direction during that time interval. The measured phase difference shows an ambiguity cycle of 2π that corresponds to a 2-way travel path difference of λ (the used radar wavelength). Thus, in principle, SAR Interferometry (INSAR) has the potential to detect ground surface motion phenomena with the accuracy of a small fraction of the radar wavelength (usually from 3 to 24 cm) on large areas (thousands of km^2) with high spatial resolution (up to 1m with the space borne SARs of the last generation as the German TERRASAR-X and the Italian Cosmo-SKyMed – CSK). INSAR is thus a unique remote sensing tool for mapping volcano dynamics, co-

seismic and post-seismic deformation along active faults, as well as slope instability and subsidence phenomena of different nature.

However, apart from cycle ambiguity problems, the routine use of INSAR is limited by the so called temporal and geometrical decorrelation, as well as to atmospheric artifacts. Temporal decorrelation appears where the electromagnetic signature of the targets changes with time (e.g. in presence of dense vegetation or water basins). Geometric decorrelation is generated by the target reflectivity variation as a function of the incidence angle. Finally, atmospheric heterogeneity superimposes on each SAR acquisition an atmospheric phase screen (APS) that could have the same spatial pattern (low-pass with typically 1 km decorrelation length) and amplitude of the surface deformation phenomenon under investigation (*Beauducel et al. 2000*).

The Permanent Scatterers (PS) Technique (*Ferretti et al. 2000, Ferretti et al. 2001, Kampes 2006, Hooper 2004, Berardino 2002)* developed in late nineties, is a powerful tool that overcomes the above said limitations of INSAR by simultaneously exploiting all the available SAR images gathered during repeated satellite passes (e.g. exploiting ESA, CSA, TERRASAR-X and, once available, the CSK archives).

After a short introduction to the PS Technique, recent examples of ground motion measurements showing the actual potential and accuracy of this remote sensing technique are presented in section 2. Also in this section the very first analysis of the improvement that can be achieved passing from the 20x5sqm resolution cell of C-Band SAR systems to the recently available 3x3sqm resolution X-band SARs is presented.

Finally, in the third section the results obtained by means of an INSAR data processing approach obtained by relaxing the strict conditions imposed by the PS technique are

shown together with an analysis of what it is gained and what is lost with respect to the PS Technique.

2.0 INSAR and DINSAR (Differential SAR Interferometry)

The European Space Agency (ESA) satellites ERS-1, ERS-2 and ENVISAT are collecting SAR data at C band (5.6 cm wavelength) since late 1991 along near polar orbits with a revisiting time of 35 days. Since 1995 the Canadian Space Agency (CSA) satellites RADARSAT-1 and RADARSAT-2 are collecting similar data with a revisiting time of 24 days. The Japanese Space Agency (JAXA) satellites J-ERS (till 1998) and ALOS have been collecting L band (23.6 cm wavelength) SAR images with a revisiting time of 44 and 46 days respectively. More recently, the German satellite TERRASAR-X and the Italian constellation of satellites Cosmo-SkyMed (CSK) started collecting SAR images at X band (3 cm wavelength) with a revisiting time of 11 and up to 4 days (with 4 satellites in orbit) respectively. An impressively huge archive of repeated SAR images is thus available for imaging and INSAR applications covering the entire Earth surface.

All these satellite SARs observe the same area at different times from slightly different looking angles since repeated orbits do not follow exactly the same track (due to the atmospheric drag, solar wind, etc). The distance between two orbits is called interferometer baseline and its projection perpendicular to the line of sight (LOS) is called perpendicular baseline (see Figure 1).

Figure 1

The phase difference between two SAR images is called interferometric phase. The following expression of the interferometric phase with respect to a selected ground reference point holds (*Ferretti et al. 2007*):

$$\Delta\phi = \frac{4\pi}{\lambda}\frac{B_n}{R\sin\theta}h + \frac{4\pi}{\lambda}\frac{B_n}{R\tan\theta}s + \frac{4\pi}{\lambda}d + \Delta\phi_{APS} + \Delta\phi_{\gamma} \qquad \text{[Eq. 1]}$$

In Eq.1, h is the relative ground elevation of targets referred to a horizontal reference plane, s is the relative slant range position of targets, d is the projection along the LOS of the relative displacement of targets, B_n is the perpendicular baseline, R is the SAR-target distance, θ is the "off-nadir" angle of the LOS, $\Delta\phi_{APS}$ is the differential tropospheric delay phase contribution (Atmospheric Phase Screen) and $\Delta\phi_{\gamma}$ is the phase noise that depends on temporal and geometric decorrelation of targets.

The first two phase terms in Eq.1 can be computed and eliminated if a precise DEM is available together with precise orbital information (baseline, sensor-target distance and off-nadir angle). The residual phase component, the so called Differential SAR Interferometric (DINSAR) phase, is then proportional to the terrain motion component along the LOS plus atmospheric and decorrelation noise:

$$\Delta\phi_d = \frac{4\pi}{\lambda}d + \Delta\phi_{APS} + \Delta\phi_{\gamma} \qquad \text{[Eq. 2]}$$

The sensitivity of the DINSAR phase to terrain motion depends on the SAR wavelength λ since a relative displacement $d = \lambda/2$ generates a differential phase variation $\Delta\phi_d = 2\pi$. From Eq.2 it is also clear that the actual possibility of measuring the terrain motion with a precision of a small fraction of the radar wavelength is mainly limited by the atmospheric and decorrelation noise terms.

Since the incidence angle of the radar signal is usually less than 30 deg (for ERS the nominal figure is 23 deg), SAR data are usually very sensitive to vertical displacements.

In Figure 2 the INSAR phases showing the co-seismic deformation of the Bam (Iran) earthquake that occurred on Dec. 26th, 2003 are shown. In this case the terrain motion is measured with a sub-centimetre precision all over the imaged area since the decorrelation phase noise terms are really small (due to lack of vegetation and small baseline) as well as the atmospheric components (due to the particular meteo conditions).

Figure 2

In many other situations, however, both decorrelation and atmospheric phase noise are so strong to severely affect terrain motion measurement. A typical example is illustrated in Figure 3 where the INSAR phases generated with ERS images taken in one day and one year interval respectively over the area of Ancona (Italy) are shown. Looking at the one day interferogram it can be clearly seen the phase decorrelation noise in the upper part of the image that corresponds to the Adriatic Sea and almost no decorrelation in land. However, on the one year interferogram (a time span that would allow to identify a big landslide motion) also the in land area is strongly affected by phase decorrelation thus preventing ground motion measurements.

Figure 3

It is interesting to note, however, that many targets that are not affected by decorrelation noise could be present in areas showing an apparent complete decorrelation as on the right image of Figure 3, but they cannot be identified since surrounded by noisy phases. The simple visual experiment illustrated in Figure 4 shows that up to 10% of randomly distributed perfectly phase coherent pixels cannot be identified when surrounded by totally random phase pixels.

Figure 4

In general, isolated phase coherent targets can be identified if more SAR scenes gathered over the area of interest are jointly analyzed. Moreover, creating many interferograms, it is usually possible to highlight problems related to spurious phase components due to DEM errors, noise and/or atmospheric signals and try to separate the different contributions. This is exactly the idea which underlies the "PS technique".

2.1 Moving from INSAR to PS

As long as a significant number and density of independent radar-phase stable points (i.e., Permanent Scatterers) exist within a radar scene and enough radar acquisitions have been collected, displacement time series and range-change rates can be calculated. Using the PS method, we can resolve surface motions at a level of ~0.5 mm/yr at about 1km from the reference point and can resolve very small-scale features, including motions of individual targets/structures (e.g. a bridge or a dam), not previously recognized in traditional SAR interferometry (*Ferretti 2007, Adam 2009*).

The PS approach is based on a few basic observations. There are ground targets that maintain a coherent reflectivity to the radar in time even when observed from different looking angles (the Permanent Scatterers - PS). The interferometric phase in correspondence of these targets is not randomized by temporal and geometric decorrelation phenomena. The PSs can be identified by a statistical analysis of amplitudes and phases of a series of SAR images gathered at different times from slightly different looking angles (the larger the number of images the more reliable is the statistical analysis). Atmospheric phase artefacts show a strong spatial correlation within every single SAR acquisition, but they are uncorrelated in time. Conversely, the phase term due to the target motion is usually strongly correlated in time and can exhibit different degrees of spatial correlation depending on the phenomenon at hand (e.g. subsidence due to water pumping, fault displacements, localized sliding areas, collapsing buildings, etc.). Finally the topographic phase term shows a linear behaviour with the normal baseline (as seen from Eq.1).

Thus, the phase terms coming from motion, atmosphere and topography can be estimated and separated from the others in correspondence of the PS locations by looking for their different behaviour in space and time.

Due to the high spatial correlation of the APS, even a low density of PS (3-4 PS/km^2) allows proper sampling of the atmospheric components. On each PS sub-metre elevation accuracy (due to the wide dispersion of the incidence angles available, usually 70 millidegrees with respect to the reference orbit) and millimetric terrain motion detection (due to the high phase coherence of these scatterers) can be achieved, once APS's are estimated and removed. In particular, relative target LOS velocity can be estimated with

184 accuracy often better than 0.5 mm/yr, due to the long time span. The higher the accuracy
185 of the measurements, the more reliable the differentiations between models of the
186 deformation process under study, a key issue for landslide monitoring and risk
187 assessment.
188 The final results of this multi-interferogram approach are the following:
189 • a map of the PS identified in the image and their coordinates;
190 • their average LOS velocity (in mm/yr);
191 • the estimated motion component of each PS as a function of time (in mm)
192 • the estimated Atmospheric Phase Delay along the LOS for every acquisition date
193

194 **2.2 PS Data Precision**

195 In the PS technique all the interferograms used in the processing are generated with
196 respect to a single master scene, properly selected among all the available SAR
197 acquisitions so that geometrical and temporal decorrelation phenomena are kept to a
198 minimum. This strategy does not allow the exploitation of radar targets exhibiting PS
199 behaviour only on a sub-set of images (as it will be discussed in Section 3), however, it
200 allows:
201 i - the exploitation of all the available SAR images (thus maximizing the temporal
202 sampling rate of the PS motion time series);
203 ii – the exploitation of large baselines (thus getting precise 3D PS positioning that is
204 essential for estimating the atmospheric delay)
205 iii – the direct sampling of the actual PS motion time series.

Moreover, it allows a first-order precision assessment of PS results using standard procedures, e.g. the computation of the *a posteriori* standard deviations of the PS velocity and elevation values. In Table 1 the typical precision of PS results obtained processing C-band data acquired by a multi-year ESA-ERS data-set is reported. It should be pointed out that new high resolution X band sensors can achieve actually better performance in both geocoding accuracy and sensitivity to target motion, nevertheless figures are noticeable and justify why InSAR data are gaining importance in space geodetic applications (*Hilley et al. 2004, Dixon et al. 2006, Ferretti et al. 2004, Berardino 2002, Kampes 2006, Hooper 2004, Ferretti 2007*)

***Table** 1*

Although a thorough statistical analysis of PS measurements is beyond the scope of this paper, it is worth pointing out that the characterization of the precision of a PS velocity field using just one statistical figure (e.g. the maximum standard deviation value within the area of interest) can be misleading. Since the precision strongly depends on the distance between the PS under study and the reference radar benchmark used in the analysis, it is actually the *variogram* (or the autocorrelation function) of the phase components that can provide a more comprehensive statistical characterization of the results.

As a rule of thumb, in any DInSAR analysis, low-frequency spatial components of the deformation pattern (such as glacial rebound effects) are always more difficult to estimate than local features (such as a landslide). In fact, both atmospheric effects and orbital fringes, i.e. the main noise sources in PSInSAR analysis apart from phase unwrapping

errors, are characterized by high spatial correlation, since their correlation length typically exceeds 1 km. Locally, spurious phase components are compensated for by the double difference computation inherent in any DInSAR analysis, but regional signals affecting hundreds or even thousands of square kilometres can be difficult to discriminate without prior information. That is the reason why PSInSAR and GPS are complementary data that can be used in synergy to map surface deformation phenomena. Indeed, geodetic observations from a few permanent GPS stations within the area of interest (a satellite frame is typically 100x100 km^2 wide) can be used successfully to calibrate PS data (all PS data a referred to a PS supposed motionless) and remove systematic errors in SAR observations (e.g. orbital components).

If no prior information is available for the area under study, the use of many data-sets coming from different acquisition geometries (ascending, descending orbits, parallel tracks, etc.) or even multi-platform analyses can help clarifying the scenario and improving the quality of the results.

2.3 The effect of resolution improvement

The ESA-ERS archive, historically, was the first one to be exploited for PSInSAR analyses. The two ERS platforms followed by ENVISAT, operating at C-band and sharing a 35-day repeat cycle, created an historical archive of SAR acquisitions since 1991, when the ERS-1 platform was successfully launched. Since then, an ever growing archive of SAR data with a spatial resolution of about 20x5 m became available and made it possible the development of many algorithms and techniques to exploit phase information (ESA archives can be found at http://earth.esa.int/resources/catalogues/)

252 RADARSAT-1 archives, launched in 1995 and still operational, offer another source of
253 InSAR data at C-band with a 24-day repeat-cycle, but the availability of many acquisition
254 modes for the radar sensor has reduced significantly the average number of homogeneous
255 data-stacks for interferometric applications, although in some areas (e.g. Italy) it has been
256 carefully planned to acquire interferometric data-sets since 2003. In January 2007,
257 RADARSAT-2 was successfully launched: this should guarantee the continuation of all
258 the applications triggered by RADARSAT-1 data availability and allows the acquisition
259 of high resolution (<3 m) data at C-band.
260 Common to optical sensors, the general trend of the aerospace industry is towards SAR
261 sensors featuring an ever increasing spatial resolution and shorter temporal sampling.
262 During the last few years, four new SAR satellites operating at X-band have been
263 launched, all featuring high spatial resolution and short repeat cycles: three belong to the
264 dual-use Cosmo-SKymed constellation operated by the Italian Space Agency, and one is
265 the German TerraSAR-X. It is then reasonable to ask what will be the impact of high-
266 resolution data on PSInSAR analyses.
267 Theoretically, the X-band wavelength (λ=3 cm) is equal to about half of the C-band (the
268 band of the ERS, ENVISAT and RADARSAT satellites) resulting in a greater sensitivity
269 (approximately double) to movement, that can lead to more accurate displacement
270 measurements. Moreover, the revisiting time is much shorter (11 days for TerraSAR-X
271 and up to 4 days for the CSK constellation, rather than 24 or 35 days) and data are
272 characterized by higher spatial resolution (<3 m), making it capable of highlighting
273 details never-before visible in satellite C-band images.

Since a Permanent Scatterer usually corresponds to a scattering center dominating the radar return of a resolution cell, the probability that a pixel of a SAR image exhibits PS behavior is certainly related to the spatial resolution of the SAR data used in the analysis. In fact, the higher the resolution, the higher the probability that a certain scattering center can dominate the surrounding scatterers sharing the same resolution cell. Of course, X-band SAR interferograms over non-urban areas are more prone to temporal decorrelation phenomena than C-band or L-band data, due to the increased sensitivity of phase values to any change in scatterers distribution, but, in principle, over man-made targets or rocky areas the spatial density of PS should significantly increase with respect to lower resolution datasets. This should be expected also due to the improved orbital stability of the newer platforms, allowing lower baseline values compared to the satellite SAR sensors launched in the nineties and the shorter repeat-cycle, limiting temporal decorrelation effects, at least for interferogram generated using two successive acquisitions.

Apart from atmospheric effects, severe limitations to DInSAR applications can arise from possible phase unwrapping errors. Indeed, phase aliasing can occur more likely than at C-band and X-band results should be carefully checked for data consistency, at least in areas exhibiting low coherence values.

In order to assess the theoretical analysis summarized in the previous paragraphs, two data-stacks acquired over the same area by both RADARSAT-1 and TERRASAR-X (TSX) have been used (Table 2). The area is in the Southern part of Italy. Here 22 TSX images acquired in Strip-Map mode from April 2008 up to January 2009 (11 days revisiting time) have been processed and compared to a previous PSInSAR result

obtained from 22 RADARSAT-1 S3 (Standard Beam) data gathered from December 2006 to September 2008 (24 days revisiting time). In both cases, all PS exhibiting a temporal coherence exceeding 0.85 have been selected. This threshold has been set to limit the number of possible statistical outliers generated by random noise to less than 10^{-5} (Colesanti et al., 2003) and corresponds, in the hypothesis of phase gaussian noise, to a standard deviation of about 0.6 rad of the phase values.

Two snapshots of the results are reported in Figures 5 and 6. In general, we measured an increased PS density by a factor of 12 that can open brand new applications to PS data, such as those related to the monitoring of individual buildings and structures. In particular, looking into Figure 6, it should be noted how, passing to high resolution SAR data, the highway crossing the area from North to South, can now be accurately monitored by means of PS data.

Since no prior information was available neither on the local topography (apart from the SRTM DEM used for the generation of the differential interferograms), nor on the surface displacement field affecting the area of interest, it was not possible to carry out a quantitative precision assessment. Moreover, it should be noted that the two datasets span two different time windows, so – at least in principle – the area could be affected by different displacement fields in the two PS results.

However, the two PS datasets have been compared by computing the difference of both average displacement rates and elevation values of a set of PS pairs (one from the RADARSAT dataset and one from the TSX dataset) less than 10 m apart. The standard deviation of the difference between the estimated displacement rate was 4.6 mm/yr while for elevation values we obtained a dispersion of 5.6 m. While the first figure is in

agreement with what should be expected based on the time spans of the datasets and the impact of atmospheric components having a dispersion of 1 rad at C-band and 1.8 rad (the ratio between the two wavelengths) at X-band, the dispersion of the elevation values is higher than expected. This is almost certainly due to the fact that the PS pairs used in the comparison could belong to different parts of a building or even to two distinct structures. Moreover any geo-coding error would impact more strongly the dispersion of the elevation values rather than the average displacement rates, since the local velocity field turned out to be smooth.

It is worth mentioning that we haven't experience any particular problem in unwrapping the phase values of the X-band datastack. This is probably due to the fact that the area is not affected by severe displacement phenomena and the local topography is not rough.

Finally in Figure 7 a vertical motion time series (LOS measurements have been projected on the vertical axis) obtained by combining RADARSAT-1 and TERRASAR-X data is shown. Here a similar vertical velocity estimate dispersion can be noted together with the higher temporal sampling offered by TERRSAR-X with respect to RADARSAT-1.

Figure 5

Figure 6

Figure 7

Table 2

3.0 From point to areal motion measurements

The main drawback of the PS approach is the low spatial density of Permanent Scatterers in particular extra-urban areas where targets remain coherent to the radar observation for a limited time interval (from weeks to months). Where the same ground deformation

affects an area covered by more resolution cells and the ground motion is strongly correlated in time, the strict conditions imposed by the PS technique (i.e. long time coherence and point-wise character of the targets) can be relaxed. Wherever the above said conditions are verified, areal ground motion information can be extracted also from partially coherent targets that are not exploited by the PS technique.

3.1 Multi-master interferograms and targets life-time

In the classical PS analysis the interferometric phase is generated by referring all images to a common Master acquisition. In the normal baseline – temporal baseline space this configuration can be represented with a star graph as in Figure 8, where each point indicates one of the 84 ERS images of the area of Dossena in the Italian Alps and each connection an interferogram.

Figure 8

In this framework, the actual coherent scatterer motion is sampled at the acquisition time of all the available SAR images. Of course only targets that coherently interfere with the Master acquisition can be exploited to get meaningful measurements. These targets should be then almost point-wise dominant targets within the resolution cell (in order to maintain coherence for large normal baselines) and temporally stable along the whole acquisition time interval of the SAR images (years, in most cases). Alternative SAR images combinations have been proposed in literature trying to relax the conditions under which a target acts as a Permanent Scatterer. As an example in the Small Baseline approach (SBAS) (*Berardino et al. 2002*), the entire set of available SAR images is

367 divided into subsets of images showing a very small normal baseline thus relaxing one of
368 the target conditions requested by the Permanent Scatterers technique. As drawbacks of
369 this approach some of the available images may not be used, the resulting graph is often
370 disconnected thus preventing the correct motion measurement without an available a
371 priori model and the small baseline condition does not allow a precise target 3D location
372 in space thus preventing a good separation of elevation, motion and atmospheric phase
373 components.
374 What is proposed here is to search for the minimum best coherence graph connecting all
375 the images of the data-set, without imposing any pre-defined decorrelation model
376 (temporal or spatial), simply by maximizing the interferometric coherence. In second
377 instance, the minimum graph can also be increased by adding more connections to make
378 the estimate more robust. Figure 9 shows the obtained graphs for the same 84 SAR
379 images data-set used for generating the "star graph" of Figure 8. As visible in the picture,
380 many selected connections have small normal baselines, but not all interferograms follow
381 this rule. Moreover, the graph is connected and can change from pixel to pixel.
382 ***Figure 9***
383 During the generation of the time-baseline connection graph, the coherence of all the
384 $\frac{(N-1)N}{2}$ interferograms that can be generated with N SAR images should be analyzed.
385 From the analysis of these coherence maps it is possible to generate a map of the average
386 coherent life-time of the imaged scatterers. The map is obtained by averaging the
387 interferometric temporal baselines weighted by the corresponding interferometric
388 coherence. By using data of the ESA-ERS archive that include also the so called
389 "tandem" interferometric pairs gathered with just one day time interval, the measurable

scatterers life-time ranges between one day and some years (e.g. 10 years for the data set used in this example). In Figure 10 such a scatterer's life-time map is shown referred to the area of Dossena. The logarithmic colour scale of Figure 10 ranges from blue (1 day) to red (more than 1000 days). The red (long life time) scatterers correspond to urban and exposed rocks areas (i.e. they are good PS candidates) whereas blue scatterers remain stable just for one day and cannot be exploited for ground motion estimation (non-coherent scatterers are not colored at all). In between there are very many scatterers with a medium lifetime shorter than that of PSs, but long enough (a few months) to allow ground motion measurement. Moreover, the "birth" and "death" dates of such medium life-time scatterers belonging to a small area affected by the same surface motion are different and by combining their individual life interval, the measurable time interval of the areal ground motion can be extended up to several years.

Figure 10

The core idea of the new technique is to jointly estimate elevation and deformation trend of a given point from the complex interferometric spatial coherence. In this way, the absolute value of the spatial coherence acts as a weight in the estimation process and only coherent interferograms play a role in the retrieval of the target parameters (uncoherent ones are weighed out). Note that the set of the actually used coherent interferograms can be different from point to point. Moreover, the phase used in the estimate is filtered by the coherence estimation process. This is an advantage for distributed targets but can lead to errors in case of high density point-wise targets areas whose elevation and motion are averaged.

As an example, the average ground areal velocity of the area of Dossena measured by exploiting the above said multi-master interferograms and partially coherent targets strategy is shown in Figure 11. As a comparison the single target average ground velocity of the same area measured by means of the standard PS Technique in shown in figure 12. By comparing Figures 11 and 12, it is quite evident that the number of measurement points increases by more than one order of magnitude passing from PSs to partially coherent targets. A detailed comparison of the estimated ground velocities at the PSs locations has shown that they are often in good agreement (standard deviation around .5 mm/year), but for some cases where two or more neighbouring PSs with different velocities have been averaged during the coherence estimation step of the partially coherent targets processing.

Figure 11

Figure 12

4.0 Conclusions

The recent technological advances of multi-temporal SAR images signal processing together with the availability of new high resolution SAR sensors with a short revisiting time can be exploited to get precise surface ground motion on a high density of measurement points covering large areas. In particular it has been shown that by increasing the spatial resolution by a factor of more than 10 (passing from the C-band RADARSAT-1 data to the X-band TERRASAR ones), the density of measurement points achieved by the Permanent Scatterers Technique increases by a factor of more than 5. Moreover, in case of the Cosmo SKY-Med mission, the shorter revisiting time of this

435 new sensors constellation would allow monitoring more rapid ground deformation
436 phenomena than in the past.
437 It has also been shown that the theoretically less precise areal measurements on a higher
438 set of partially coherent targets can complement the more precise point wise scatterers
439 time series achievable with the PS Technique.
440 The integration of these techniques with other independent measurements (e.g. GPS)
441 represents a powerful tool that can be exploited by geologists and geophysicists for
442 investigating many ground deformation phenomena (*Burgmann 2006*).
443 Finally it should be pointed out that maps of the differential travel time delay are
444 generated as a side product of these techniques. These maps could be usefully exploited
445 to get information on the troposphere water vapor content with unprecedented spatial
446 resolution.
447
448 **References**
449
450 Adam N., Parizzi A., Eineder M., Crosetto M., "Practical persistent scatterer processing
451 validation in the course of the Terrafirma project", Journal of Applied Geophysics 69
452 (2009) 5965.
453
454 Bamler R., Hartl P., “Synthetic Aperture Radar Interferometry”, Inverse Problems,
455 Vol.14, R1-R14, 1998.
456

457 Beauducel, F., P. Briole, and J.-L. Froger (2000), Volcano-wide fringes in ERS synthetic
458 aperture radar interferograms of Etna (1992–1998): Deformation or tropospheric effect?,
459 *J. Geophys. Res.*, 105(B7), 16,391–16,402.
460
461 Berardino P., Fornaro G., Lanari R., and Sansosti E., "A new algorithm for surface
462 deformation monitoring based on small baseline differential interferograms," IEEE
463 Transactions on Geoscience and Remote Sensing, Vol. 40, No. 11, pp. 2375–2383, 2002.
464
465 Bürgmann R., Hilley G., Ferretti A., Novali F., "Resolving vertical tectonics in the San
466 Francisco Bay Area from permanent scatterer InSAR and GPS analysis", Geology;
467 March 2006; v. 34; no. 3; p. 221-224.
468
469 Colesanti C., Ferretti A., Novali F., Prati C., Rocca F., "SAR Monitoring of progressive
470 and seasonal ground deformation using the permanent scatterers technique," IEEE
471 Transactions On Geoscience and Remote Sensing, Vol. 41, p. 1685-1701, 2003.
472
473 Dixon T., Amelung F., Ferretti A., Rocca F., Novali F., Wdowinski S., "New Orleans
474 Subsidence and Relation to Flooding after Hurricane Katrina, as measured by Space
475 Geodesy", Nature, Vol. 441, N. 7093, June 2006, pp. 587 - 588.
476
477 Ferretti A., Prati C., Rocca F., "Nonlinear subsidence rate estimation using Permanent
478 Scatterers in differential SAR", IEEE Transactions on Geoscience and Remote Sensing,
479 Vol. 38, pp. 2202–2212, 2000.

Ferretti A., Prati C., Rocca F., “Permanent Scatterers in SAR Interferometry”, IEEE Transactions on Geoscience and Remote Sensing, Vol. 39, N.1, pp. 8–20, 2001.

Ferretti A., Monti Guarnieri A., Prati C., Rocca F., Massonnet D. “INSAR Principles: Guidelines for SAR Interferometry Processing and Interpretation”, ESA Publications, TM-19, February 2007.

Ferretti A., Novali F., Burgmann R., Hilley G., Prati C., “InSAR Permanent Scatterers Analysis Reveals Ups and Downs in San Francisco Bay Area”, EOS, Transactions, American Geophysical Union, Vol. 85, N.34, pp.317 and 324, August 2004.

Ferretti, A., Savio, G., Barzaghi, R., Borghi, A., Musazzi, S., Novali, F., Prati, C., Rocca F., “Submillimeter Accuracy of InSAR Time Series: Experimental Validation”, IEEE Transactions on Geoscience and Remote Sensing, Volume 45, Issue 5, May 2007 Page(s):1142 – 1153.

Hilley G., Burgmann R., Ferretti A., Novali F., Rocca F., “Dynamics of Slow-Moving Landslides from Permanent Scatterer Analysis”, Science, pp. 1952 - 1956, June 2004.

Hooper A., Zebker H., Segall P., Kampes B., "A new method for measuring deformation on volcanoes and other natural terrains using InSAR persistent scatterers", Geophysical Research Letters, Vol. 31, L23611, 2004.

Kampes B., "Radar Interferometry: Persistent Scatterer Technique", Springer, 2006.

504

505

506 **Figure Captions**

507 **Figure 1** - INSAR acquisition geometry.

508 **Figure 2** - Example of co-seismic interferogram of the Bam (Iran) earthquake, Dec. 26th,
509 2003 formed with 2 ENVISAT images (about 30x40km) taken before and after the
510 earthquake respectively. Each colour cycle corresponds to a relative ground displacement
511 $d = \lambda/2$ (i.e. about 2.8cm).

512 **Figure 3** - Example of interferograms of the town of Ancona (on the Adriatic Italian
513 coast) formed with ERS images taken in one day (left) and one year time interval (right)
514 respectively.

515 **Figure 4** - Left: random spatial distribution of phase coherent samples (10% of the total)
516 showing a possible terrain subsidence with a gaussian shape. Right: the image on the left
517 has been filled with random phase samples. Coherent pixels are still there, but they
518 cannot be identified visually or by means of any sort of spatial filtering.

519 **Figure 5** - Spatial distribution of the Permanent Scatterers identified in an urban area
520 located in the Southern part of Italy (an aerial orthophoto is used as background). The
521 color scale is related to PS elevation, ranging from red (sea level) to blue (50 m). Upper
522 image: PS obtained by processing 62 RADARSAT-1 S3 (Standard Beam) images
523 covering the period 2003-2007. Lower image: PS obtained by processing 22 TSX images
524 acquired in Strip-Map mode from April 2008 up to January 2009.

525 **Figure 6 –** Average Spatial distribution of the Permanent Scatterers identified in a semi-
526 urban area located in the Southern part of Italy (an aerial orthophoto is used as

background). The color scale is related to PS elevation, ranging from red (sea level) to blue (50 m). Upper image: PS obtained by processing 62 RADARSAT-1 S3 (Standard Beam) images covering the period 2003-2007. Lower image: PS obtained by processing 22 TSX images acquired in Strip-Map mode from April 2008 up to January 2009.

Figure 7 – Vertical velocity time series of a PS obtained by combining RADARSAT and TSX data.

Figure 8 - Normal baseline – temporal baseline space of 84 ERS SAR images of the area of Dossena in the Italian Alps. Each point indicates an image whose acquisition time with respect to the Master in shown in abscissa (days) and perpendicular baseline with respect to the Master in shown in ordinate (m). The Master image has coordinates (0,0) and each of the 83 connections indicates that an interferogram is formed between the Master and the remaining 83 Slave images.

Figure 9 - Normal baseline – temporal baseline space of the same 84 ERS SAR images data-set used in Figure 8. Left: 83 lines connect all the images in such a way that 83 interferograms with the highest possible coherence are generated. The colour of the connection lines indicates the estimated coherence of each interferometric pair. The minimum best coherence graph can change from pixel to pixel. Right: Some among the 3403 possible connections (i.e. higher coherence interferograms) have been added to the minimum best coherence graph.

Figure 10 - Scatterers life-time map of an area of the Italian Alps. The logarithmic colour scale ranges from blue (1 day) and is saturated to red (more than 1000 days).

Figure 11 - average ground areal velocity of the area of Dossena measured by exploiting the multi-master interferograms and partially coherent targets strategy.

Figure 12 - single target average ground velocity of the area of Dossena measured by means of the standard PS Technique

Tables

Table 1: Typical precision figures for PS results obtained by processing an ESA-ERS dataset (C-band radar data) having at least 40 scenes (35-day temporal sampling) at a distance less than 1 km from the reference PS.

Table 2: Nominal parameters values of RADARSAT-1 and TERRASAR-X data used in the comparison analyzed in the text.

Figure

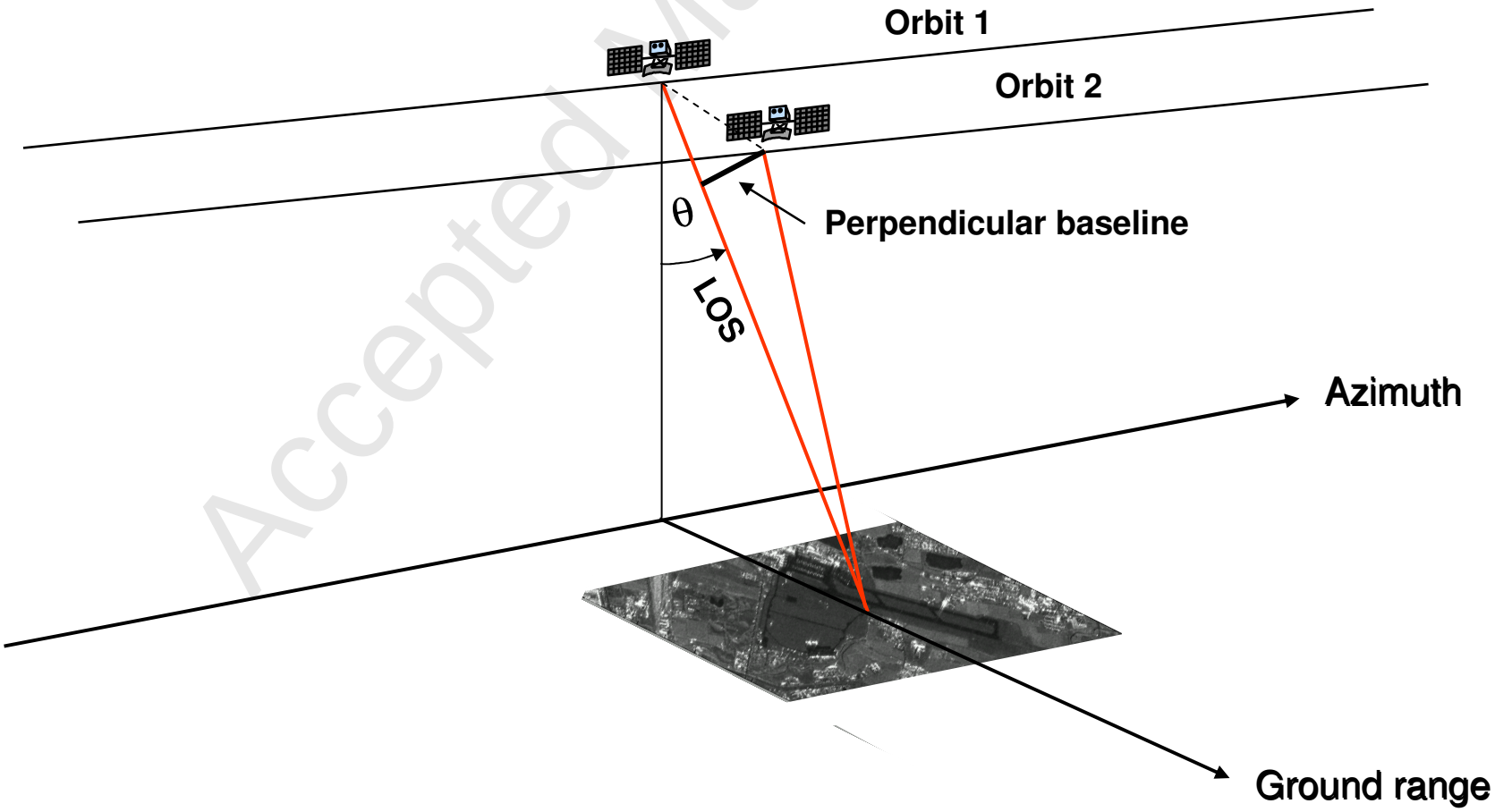

Figure

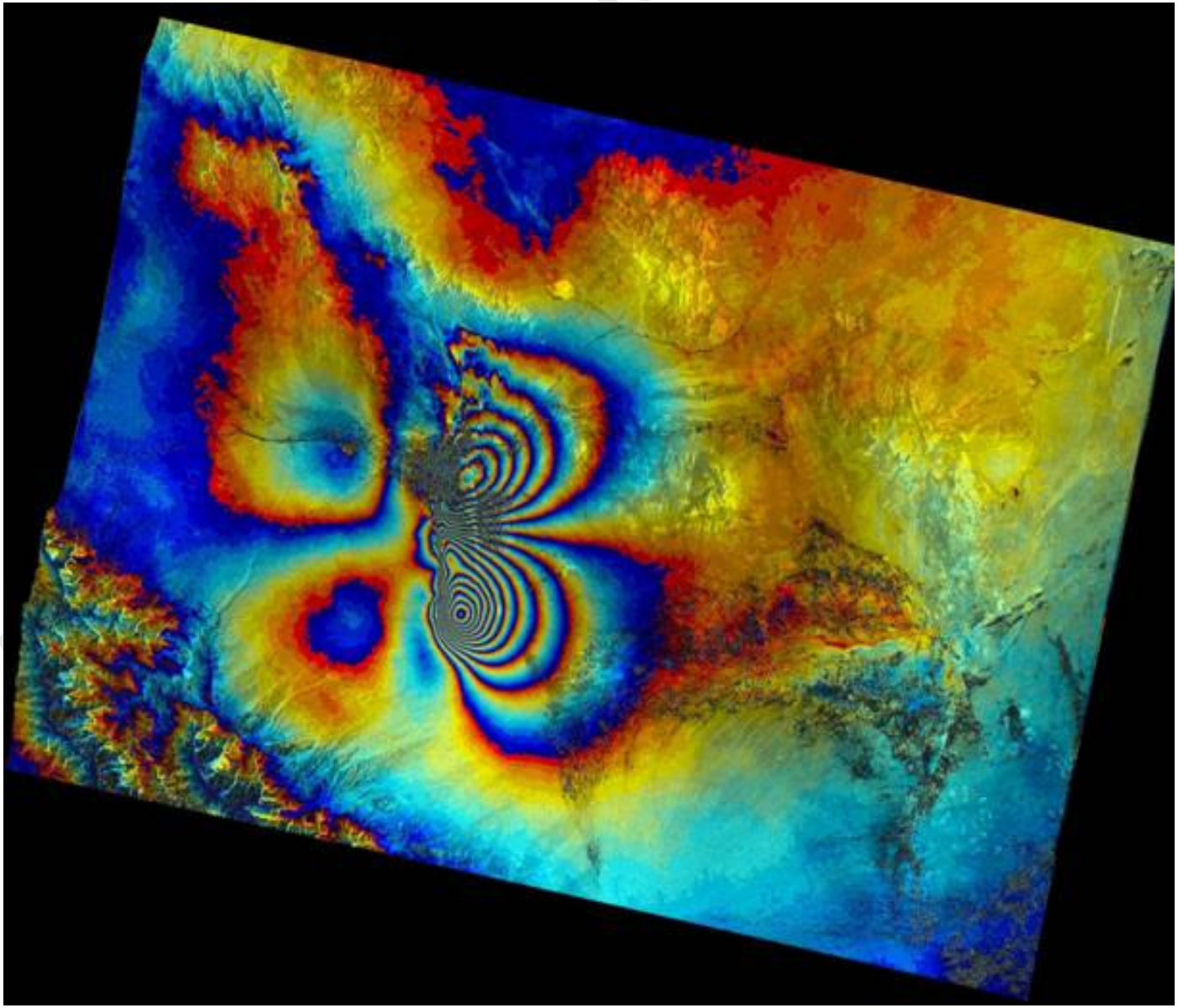

Figure

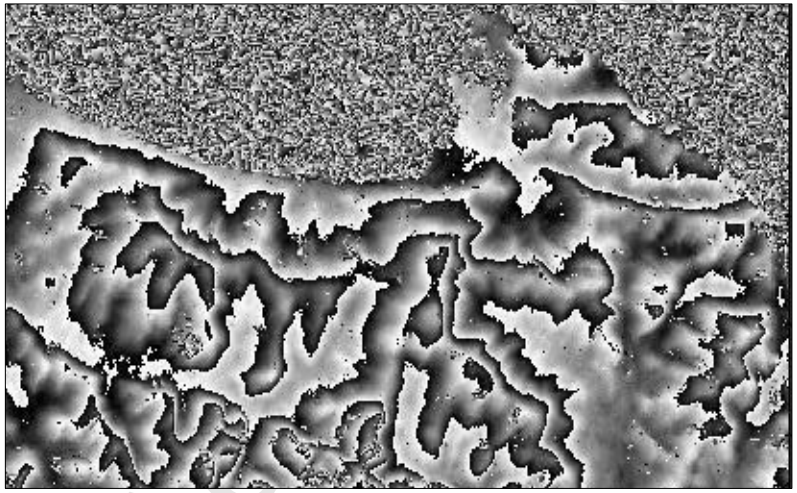

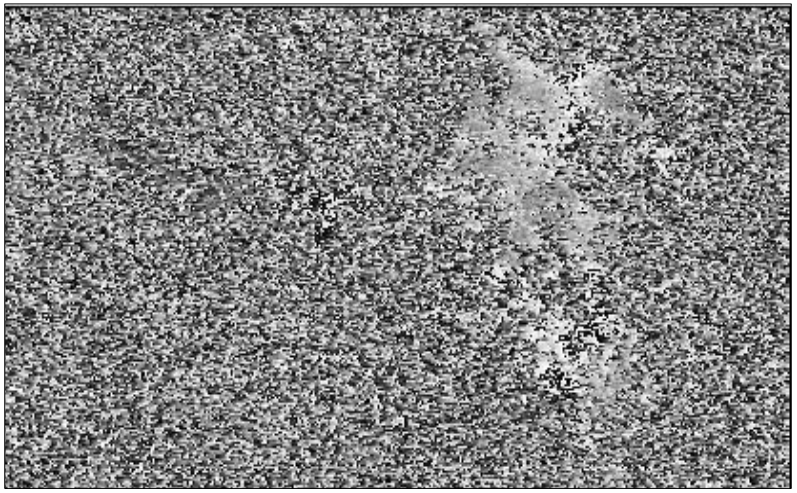

Figure

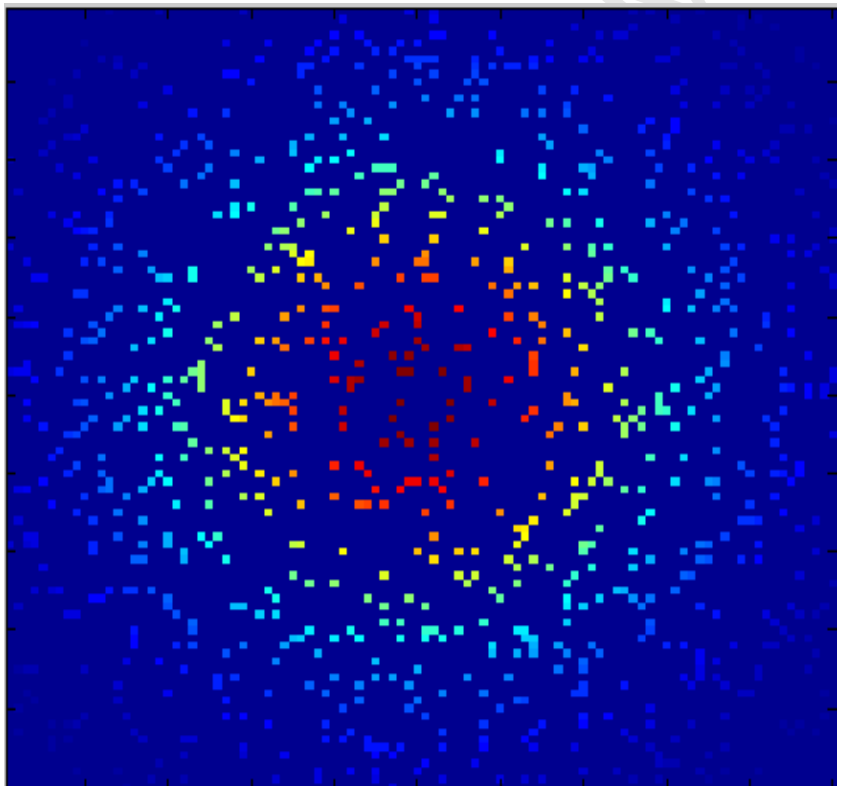

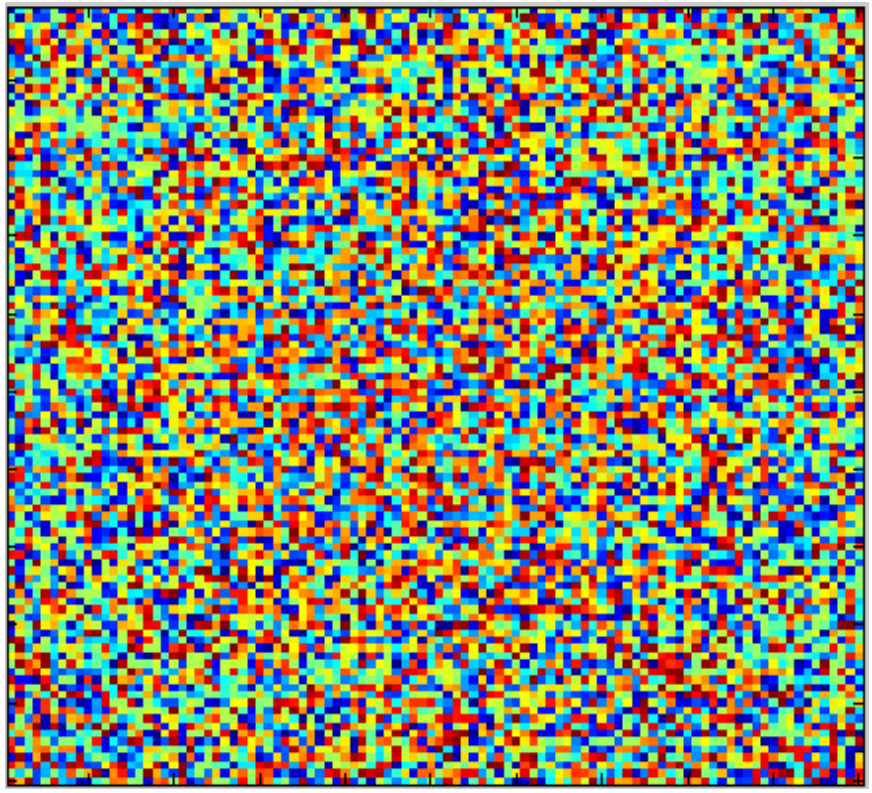

Meters
0 500 1.000

Number of Images: 22
First Acquisition: 23 Dec 2006
Last Acquisition: 07 Sep 2008

PSInSAR™ Analysis
RSAT-1 Descending Data

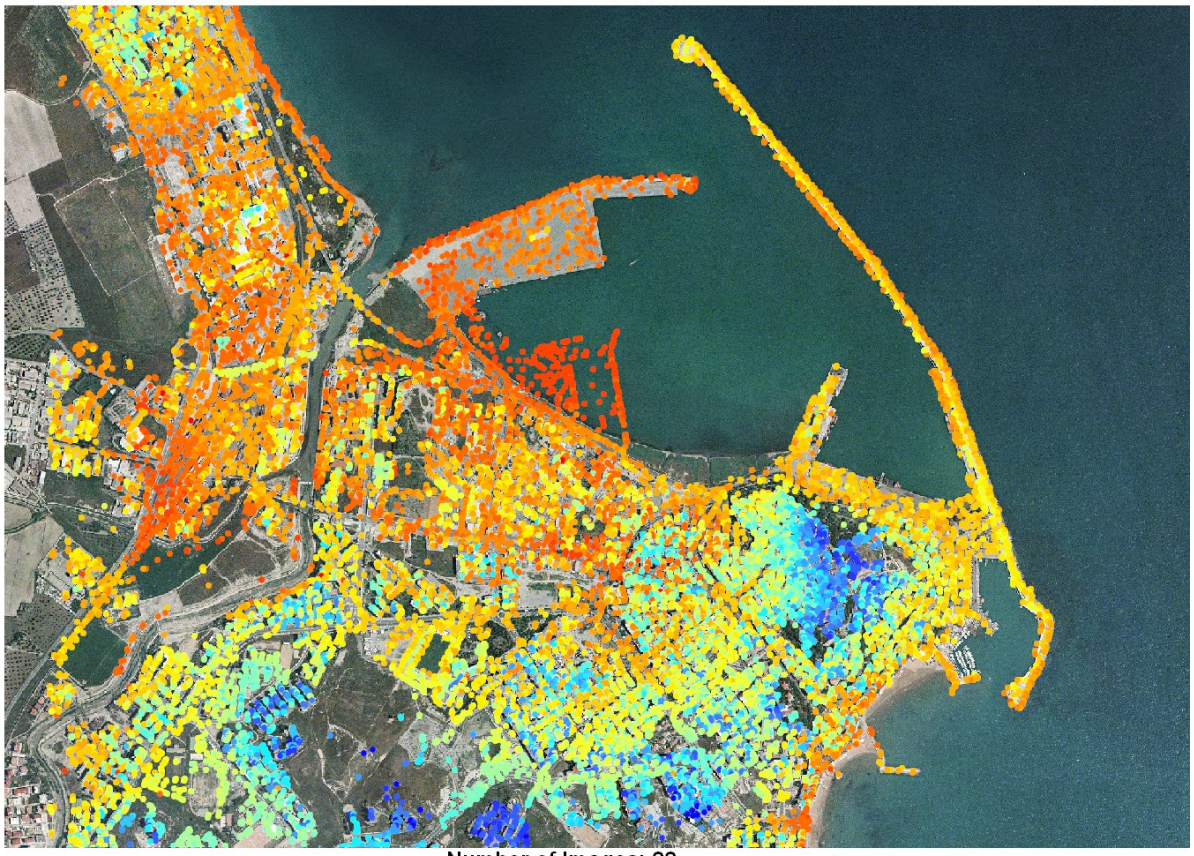

Meters
0 500 1.000

Number of Images: 22
First Acquisition: 25 Apr 2008
Last Acquisition: 14 Jan 2009

PSInSAR™ Analysis
TerraSAR-X Descending Data

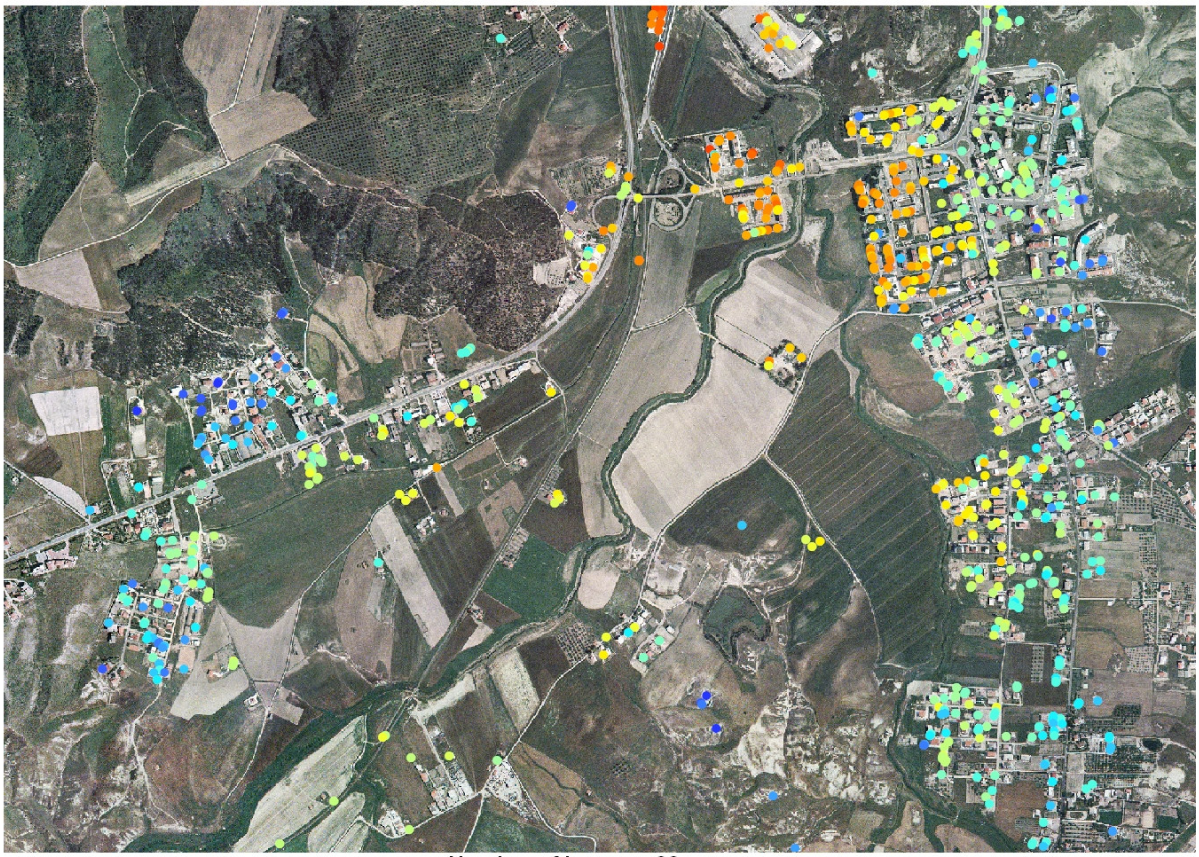

Meters
0 500 1.000

Number of Images: 22
First Acquisition: 23 Dec 2006
Last Acquisition: 07 Sep 2008

PSInSAR™ Analysis
RSAT-1 Descending Data

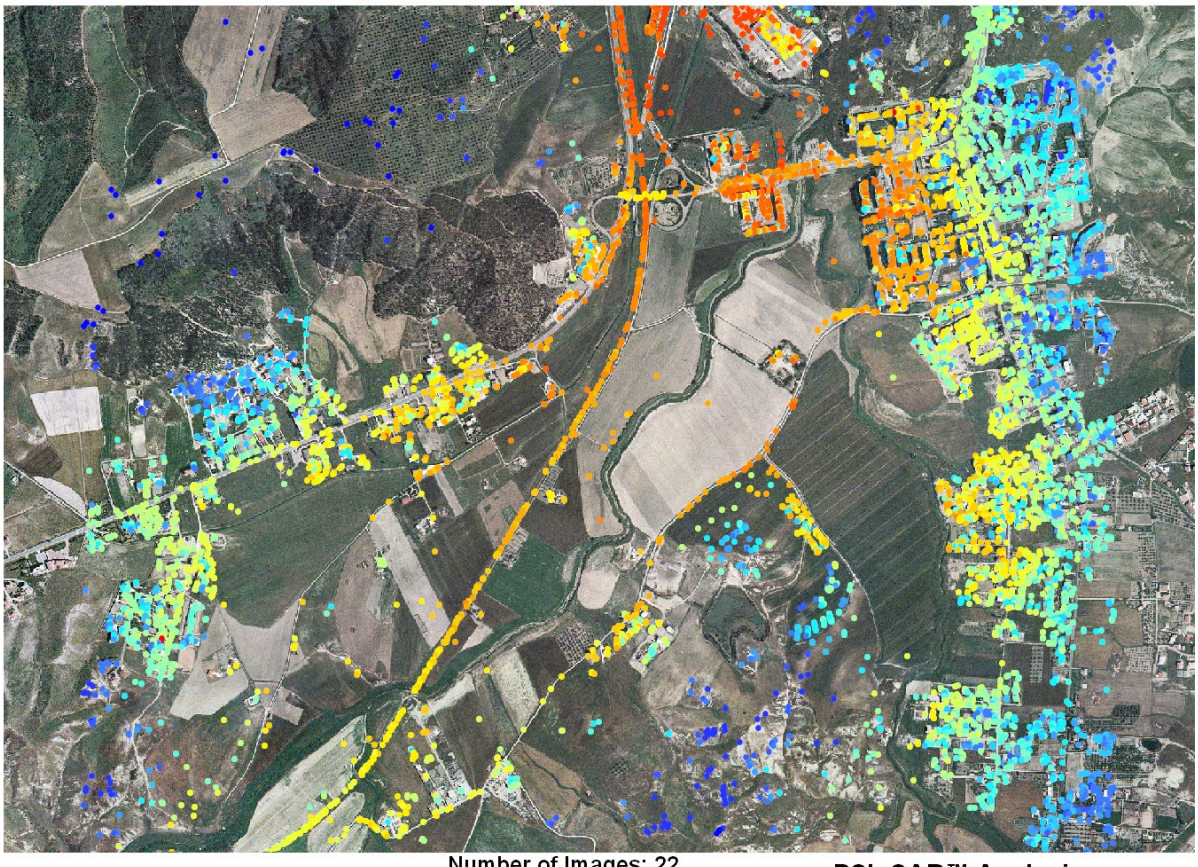

Meters
0 500 1.000

Number of Images: 22
First Acquisition: 25 Apr 2008
Last Acquisition: 14 Jan 2009

PSInSAR™ Analysis
TerraSAR-X Descending Data

Figure

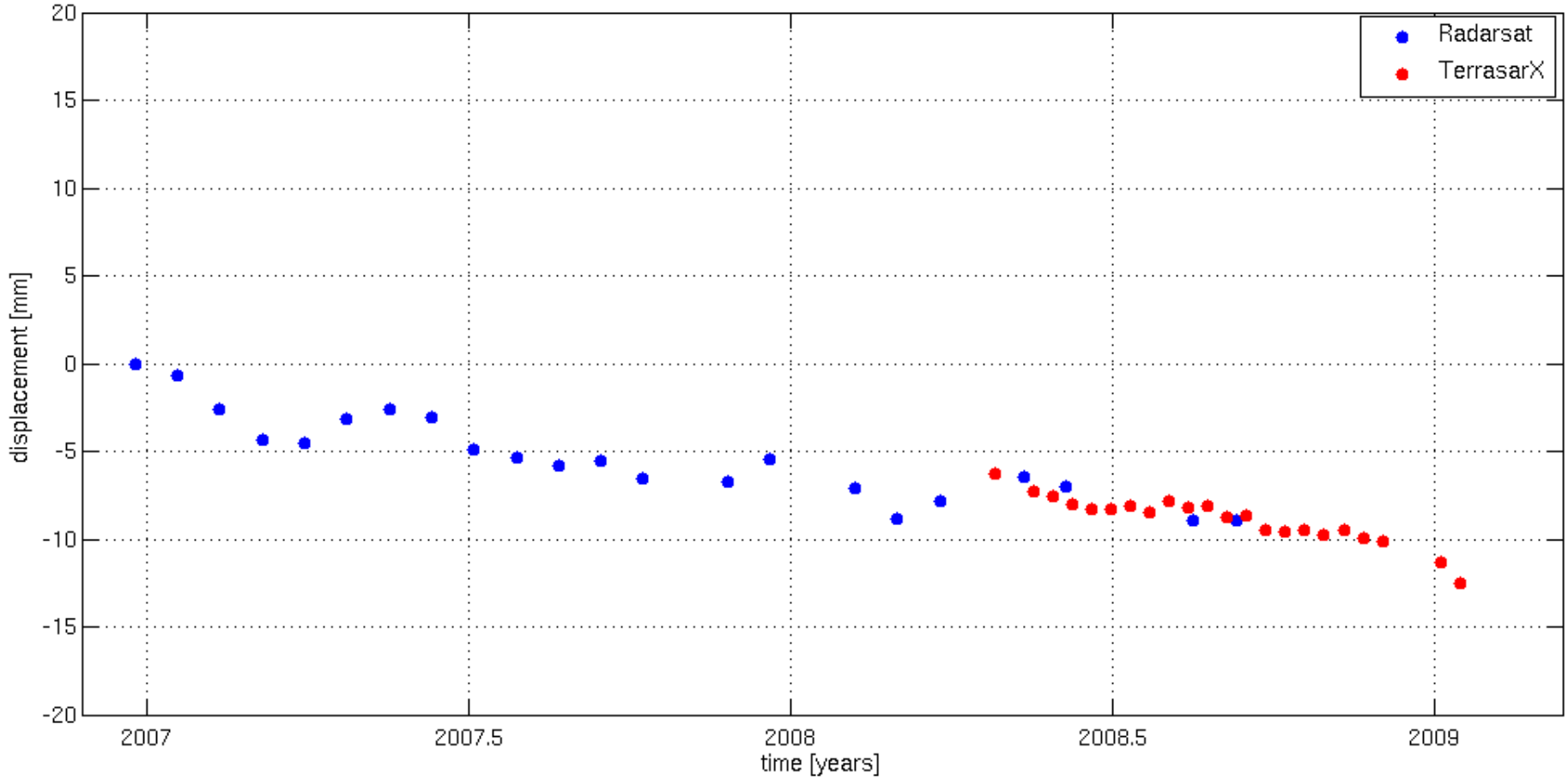
Radarsat
TerrasarX
displacement [mm]
time [years]
20
15
10
5
0
-5
-10
-15
-20
2007
2007.5
2008
2008.5
2009

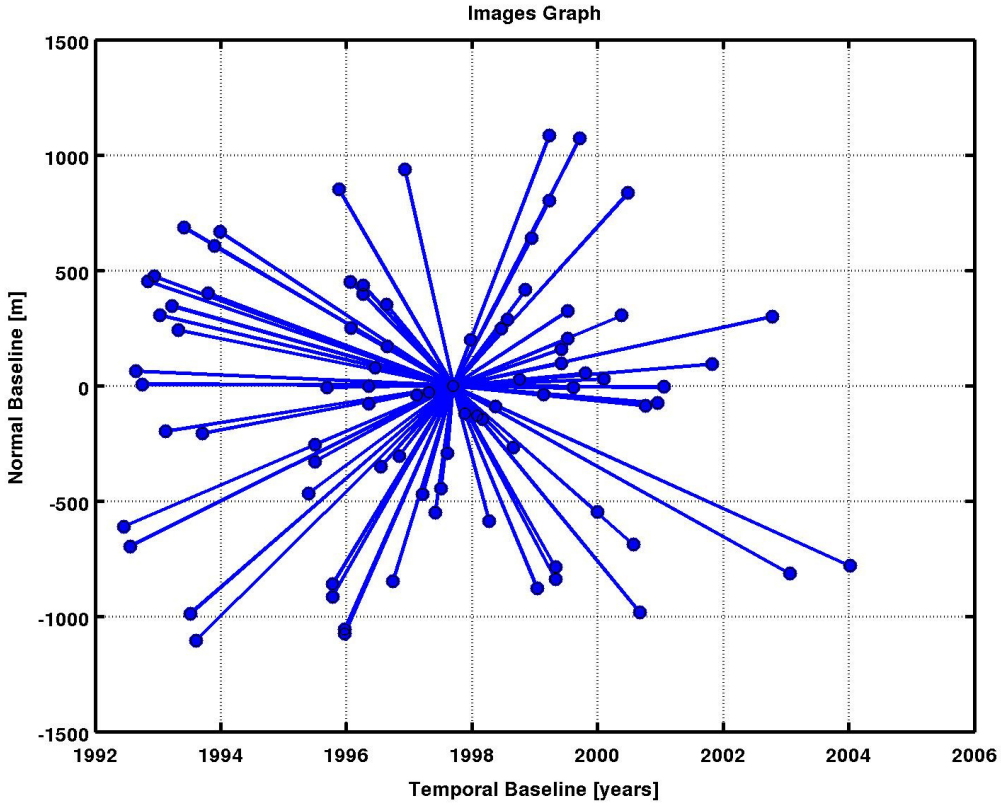
Images Graph
Normal Baseline [m]
Temporal Baseline [years]
1500
1000
500
0
-500
-1000
-1500
1992
1994
1996
1998
2000
2002
2004
2006

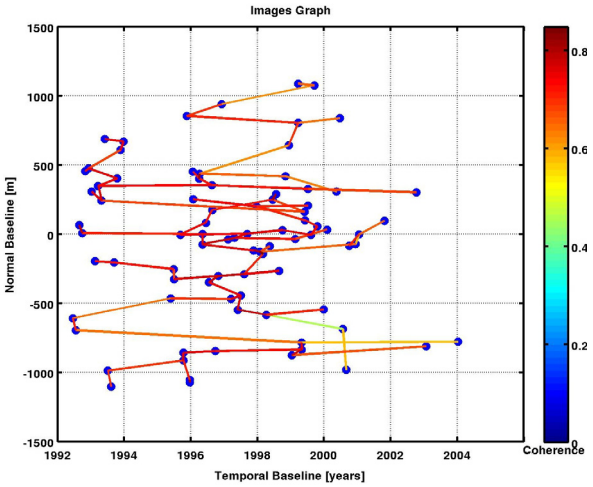
Images Graph
Normal Baseline [m]
Temporal Baseline [years]
Coherence
1500
1000
500
0
-500
-1000
-1500
1992
1994
1996
1998
2000
2002
2004
0.8
0.6
0.4
0.2
0

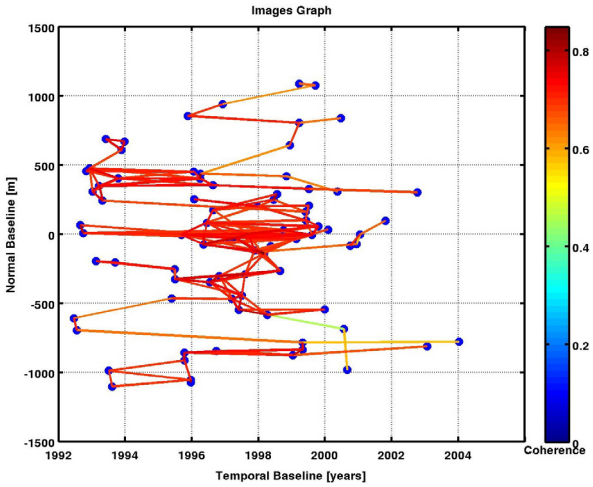
Images Graph
Normal Baseline [m]
Temporal Baseline [years]
Coherence
1500
1000
500
0
-500
-1000
-1500
1992
1994
1996
1998
2000
2002
2004
0.8
0.6
0.4
0.2
0

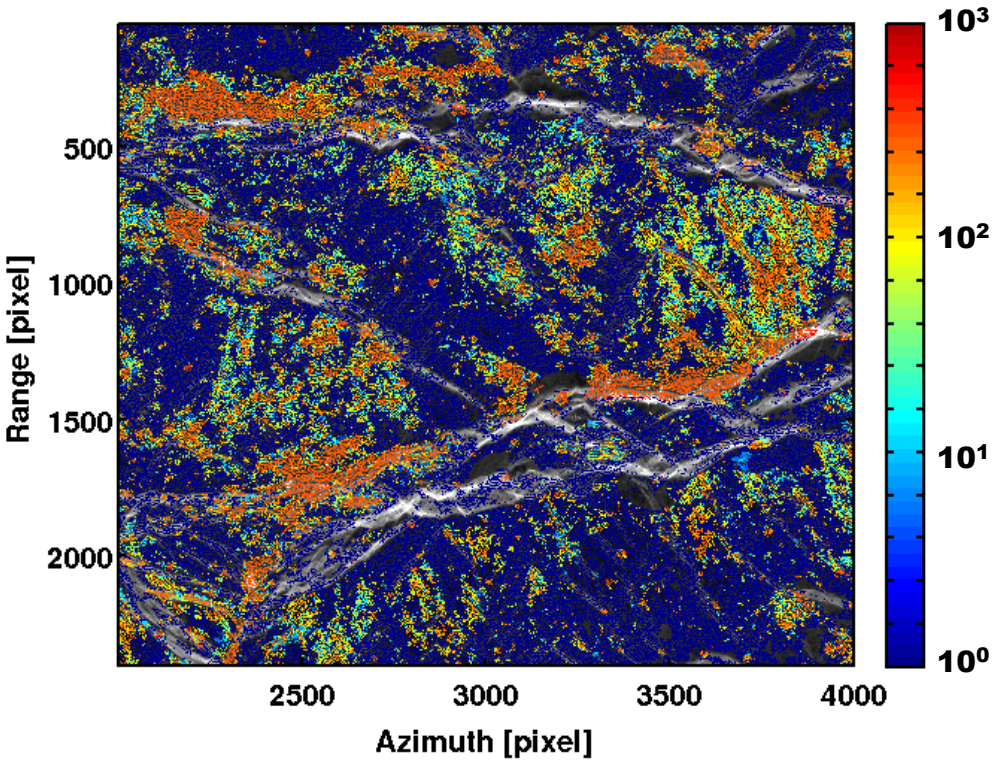
Range [pixel]
500
1000
1500
2000
2500
3000
3500
4000
Azimuth [pixel]
10^3
10^2
10^1
10^0

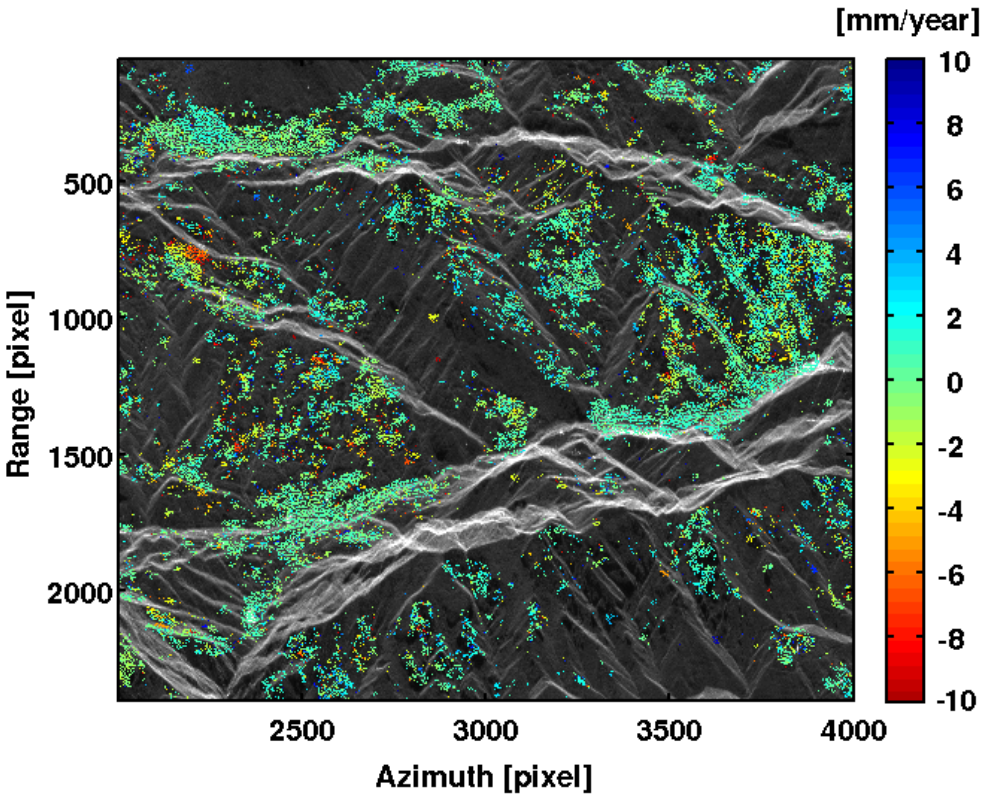
[mm/year]
10
8
6
4
2
0
-2
-4
-6
-8
-10
Range [pixel]
500
1000
1500
2000
2500
3000
3500
4000
Azimuth [pixel]

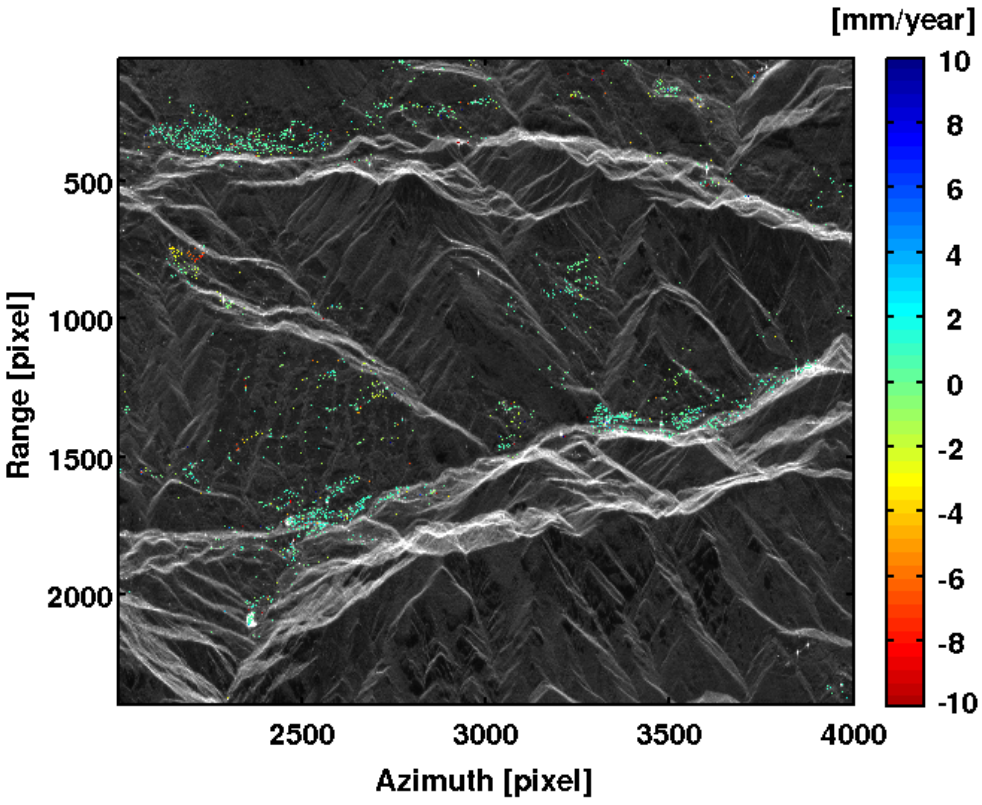
[mm/year]
10
8
6
4
2
0
-2
-4
-6
-8
-10
500
1000
1500
2000
Range [pixel]
2500
3000
3500
4000
Azimuth [pixel]

	Precision (1 σ)
Easting	<5 m
Northing	<2 m
Height	<1 m
Displacement Rate	<0.5 mm/yr
Single Displacement Measurement	<5 mm

	RADARSAT-1	TERRASAR-X
Acquisition Mode	Standard Beam - S3	Strip-map -SM
Orbit	Descending	Descending
Incidence angle	37 deg	29 deg
Bandwidth	11.6 MHz	150 MHz
Wavelength	5.6 cm	3.1 cm
Pixel posting (azimuth)	5.1 m	2.1 m
Pixel posting (range)	11.6 m	0.9 m
Polarization	HH	HH